

The elusive actin cytoskeleton of a green alga expressing both conventional and divergent actins

Evan W. Craig^a, David M. Mueller^a, Brae M. Bigge^a, Miroslava Schaffer^b, Benjamin D. Engel^b, and Prachee Avasthi^{a,c,*}

^aDepartment of Anatomy and Cell Biology and ^cDepartment of Ophthalmology, University of Kansas Medical Center, Kansas City, KS 66160; ^bDepartment of Molecular Structural Biology, Max Planck Institute of Biochemistry, 82152 Martinsried, Germany

ABSTRACT The green alga *Chlamydomonas reinhardtii* is a leading model system to study photosynthesis, cilia, and the generation of biological products. The cytoskeleton plays important roles in all of these cellular processes, but to date, the filamentous actin network within *Chlamydomonas* has remained elusive. By optimizing labeling conditions, we can now visualize distinct linear actin filaments at the posterior of the nucleus in both live and fixed vegetative cells. Using in situ cryo-electron tomography, we confirmed this localization by directly imaging actin filaments within the native cellular environment. The fluorescently labeled structures are sensitive to the depolymerizing agent latrunculin B (Lat B), demonstrating the specificity of our optimized labeling method. Interestingly, Lat B treatment resulted in the formation of a transient ring-like filamentous actin structure around the nucleus. The assembly of this perinuclear ring is dependent upon a second actin isoform, NAP1, which is strongly up-regulated upon Lat B treatment and is insensitive to Lat B-induced depolymerization. Our study combines orthogonal strategies to provide the first detailed visual characterization of filamentous actins in *Chlamydomonas*, allowing insights into the coordinated functions of two actin isoforms expressed within the same cell.

Monitoring Editor
Thomas D. Pollard
Yale University

Received: Mar 7, 2019
Revised: Sep 6, 2019
Accepted: Sep 10, 2019

INTRODUCTION

Actin is a highly conserved protein that is essential for survival in most eukaryotic cells (Pollard *et al.*, 2000). In yeast, the only actin isoform makes distinct structures such as actin patches, cables, and cytokinetic rings (Kilmartin and Adams 1984; Warren *et al.*, 2002). These structures function in endocytosis, organelle and protein transport, and cell division, respectively. Unlike yeast, mammalian cells have six different actin isoforms encoded by six separate genes. These function collectively to regulate cell morphology,

motility, mechanotransduction, membrane dynamics, and intracellular trafficking. Some of these functions require complex interactions between actin isoforms, and single actin knockout studies in mice revealed that loss of one gene causes a compensatory up-regulation of a subset of the remaining actin isoforms (Perrin and Ervasti, 2010).

The genome of the unicellular green alga *Chlamydomonas reinhardtii* contains two actin genes that vary significantly in sequence. Inner dynein arm 5 (IDA5) is a highly conserved conventional actin, whereas novel actin-like protein 1 (NAP1) is a divergent actin that only shares ~65% sequence identity with mammalian actin (Kato-Minoura *et al.*, 1997; Onishi *et al.*, 2016). Genetic loss of IDA5, a condition in which NAP1 is expressed at low levels, results in slow swimming (Ohara *et al.*, 1998) and early ciliary growth defects due to reduced ciliary protein accumulation and entry (Avasthi *et al.*, 2014). Ciliary growth ultimately proceeds and can reach normal length. However, when both actins are disrupted acutely, *Chlamydomonas* cells show dramatic defects in ciliary protein synthesis, vesicular trafficking, and organization of a key gating region dictating ciliary protein composition (Jack *et al.*, 2019). Given

This article was published online ahead of print in MBoC in Press (<http://www.molbiolcell.org/cgi/doi/10.1091/mbc.E19-03-0141>) on September 18, 2019.

*Address correspondence to: Prachee Avasthi (pavasthi@kumc.edu).

Abbreviations used: CHX, cycloheximide; cryo-ET, cryo-electron tomography; DAPI, 4',6-diamidino-2-phenylindole; IDA5, inner dynein arm 5; Lat B, latrunculin B; NAP1, novel actin-like protein 1; PAM, peptidylglycine alpha-amidating monooxygenase; PBS, phosphate-buffered saline; PFA, paraformaldehyde.

© 2019 Craig *et al.* This article is distributed by The American Society for Cell Biology under license from the author(s). Two months after publication it is available to the public under an Attribution–Noncommercial–Share Alike 3.0 Unported Creative Commons License (<http://creativecommons.org/licenses/by-nc-sa/3.0>).

“ASCB®,” “The American Society for Cell Biology®,” and “Molecular Biology of the Cell®” are registered trademarks of The American Society for Cell Biology.

that *ida5* mutants expressing NAP1 alone do not show these defects, it appears NAP1 can largely perform the actin-dependent functions needed for ciliary assembly despite its sequence divergence with IDA5. Although we have been able to genetically and chemically dissect the functions of the individual actin isoforms, detailed visual characterization of filamentous actin networks has eluded the field.

Although actin filaments are readily visualized by traditional phalloidin staining in mammalian systems, a variety of protein and cellular differences complicate actin visualization in protists and highlight the need for labeling optimization in different cellular systems. In the parasite *Toxoplasma gondii*, the actin gene *ACT1* shares 83% sequence identity with mammalian actin and is required for cell motility, yet filamentous actin is undetectable by phalloidin staining (Dobrowolski *et al.*, 1997). Other conventional filamentous actin labeling techniques such as LifeAct and SiR-actin also fail to label filamentous actin in this parasite (Periz *et al.*, 2017). This may be due to the highly dynamic filament turnover and distinct actin polymerization kinetics (Miraldi *et al.*, 2008) found in *T. gondii* and closely related *Plasmodium falciparum*. Biochemical assays also show that 97% of the parasites' actin exists in globular form (Dobrowolski *et al.*, 1997; Wetzal *et al.*, 2003; Skillman *et al.*, 2011), creating unfavorable conditions for filamentous actin staining. As in parasitic protists, *Chlamydomonas* actin visualization with conventional strategies has been challenging. Actin antibodies do not discriminate between filamentous and monomeric actin, and previous attempts to visualize the filamentous actin cytoskeleton using fluorescent phalloidins resulted in a diffuse signal throughout the cytoplasm in vegetative *Chlamydomonas* cells (Harper *et al.*, 1992), leading some to conclude that these cells made few, if any, filaments (Harper *et al.*, 1992). The only condition where phalloidins have been shown to clearly label filamentous actin in *Chlamydomonas* is in gametes, where filamentous actin-rich tubules can be seen at the apical surface between the flagella upon mating or artificial induction (Detmers *et al.*, 1985).

Advancements in vegetative *Chlamydomonas* actin filament visualization came from live-cell imaging using strains expressing the fluorescently tagged filament binding peptide, LifeAct (Avasthi *et al.*, 2014; Onishi *et al.*, 2016). This method identified linear structures at the posterior of the nucleus and less frequently at the base of the flagella. Acute treatment with the actin-depolymerizing agent latrunculin B (Lat B) eliminated this labeling (Avasthi *et al.*, 2014; Onishi *et al.*, 2016), demonstrating the specificity of the fluorescent LifeAct for actin filaments.

However, longer incubation with Lat B restored a partial signal with a slightly different distribution (Onishi *et al.*, 2016). This new signal likely represents the Lat B-induced up-regulation of a second *Chlamydomonas* actin normally expressed at low levels, the novel actin-like protein NAP1 (Kato-Minoura *et al.*, 1998; Onishi *et al.*, 2016). Despite the identification of a clear filamentous actin-based perinuclear structure using fluorescent LifeAct, technical challenges to maintaining LifeAct expression and the inability to preserve labeled structures in fixed cells for colocalization with cellular organelles required a different method of actin visualization.

We reasoned that *Chlamydomonas* actin, IDA5, which shares 90% sequence identity with mammalian actins, is inherently capable of binding fluorescent phalloidins due to the intense staining of fertilization tubules in gametes. For this study, we developed an optimized protocol for phalloidin staining that recapitulated LifeAct labeling (Craig and Avasthi, 2019). Using this method, and corroborating with live-cell visualization and cryo-electron tomography (cryo-ET), we can now show for the first time how actin filaments

are localized and dynamically redistributed in vegetative and gametic *Chlamydomonas* cells. In addition, we applied this staining method to mutants of each actin isoform to reveal new insights into isoform-specific organization and function.

RESULTS

Filamentous actin visualization in vegetative *Chlamydomonas* achieved by an optimized phalloidin staining protocol

To optimize phalloidin labeling, which previously produced only a weak, diffuse, seemingly nonspecific signal in vegetative cells (Figure 1, A, C, and E; Harper *et al.*, 1992), we used a combination of bright and photostable Atto fluorophores and reduced incubation times to limit background fluorescence. Specifically, reducing incubation to 16 min was crucial to successful staining. We also improved the imaging by employing deconvolution microscopy to remove out-of-focus light. Using this optimized protocol (Craig and Avasthi, 2019), we found that the pattern of phalloidin staining matched what was seen for LifeAct-Venus fluorescence, with a tangle of linear filaments at the posterior of the nucleus (Figure 1, B, D, and F), providing further support that the previously identified midcell LifeAct signal (Avasthi, *et al.*, 2014; Onishi *et al.*, 2016) represents the filamentous actin population. Phalloidin-labeled structures were disrupted when treated with the actin-depolymerizing drug, Lat B (Figure 2).

With a newly developed method for actin labeling *Chlamydomonas* cells, we tested the ability of Atto 488 phalloidin to costain with probes for other cytoskeletal proteins (Figure 3). Filamentous actin was observed in the midcell region (Figure 3A), and costaining with 4',6-diamidino-2-phenylindole (DAPI), a DNA label, we observed localization posterior to the nucleus with occasional threads linking to a region near the apical flagellar base (Figure 3B). Atto 488 phalloidin costained efficiently with centrin antibodies, which mark the basal bodies and fibers connecting to the nucleus (Figure 3C), as well as α -tubulin antibodies, which stain microtubules in the cilia, basal bodies, and cell body (Figure 3D).

In situ cryo-electron tomography of actin filaments

To directly visualize actin filaments within the native cellular environment, we rapidly froze vegetative *Chlamydomonas* cells in vitreous ice, thinned these cells by focused ion beam milling, and then imaged them by cryo-ET (Asano *et al.*, 2016). Helical filaments with a diameter of ~ 7 nm (consistent with filamentous actin) were observed in the cytosol at the posterior side of the nucleus, near the nuclear envelope, endoplasmic reticulum, and Golgi (Figure 4). In addition to relatively straight individual actin filaments (Figure 4, A and B), we also observed loosely tangled bundles of filaments with increased local curvature (Figure 4C).

Reorganization of filaments during gamete induction

Our optimized staining protocol allowed us to compare actin filament localization across *Chlamydomonas* cell states. Vegetative and gametic cells displayed similar perinuclear actin localization. Interestingly, gametic cells often showed a single apical fluorescent spot between the two flagella (Figure 5B, inset). In the case of vegetative cells, this apical fluorescence was observed much less frequently and formed one, two, three, or four spots. Even in synchronous cultures, no consistent apical staining pattern was observed. The apical filamentous actin foci in gametes may mark the location of eventual fertilization tubule formation before induction in mating type plus CC-125 cells. To test this hypothesis, we asked whether mating type minus CC-124 cells, which do not make fertilization tubules, have

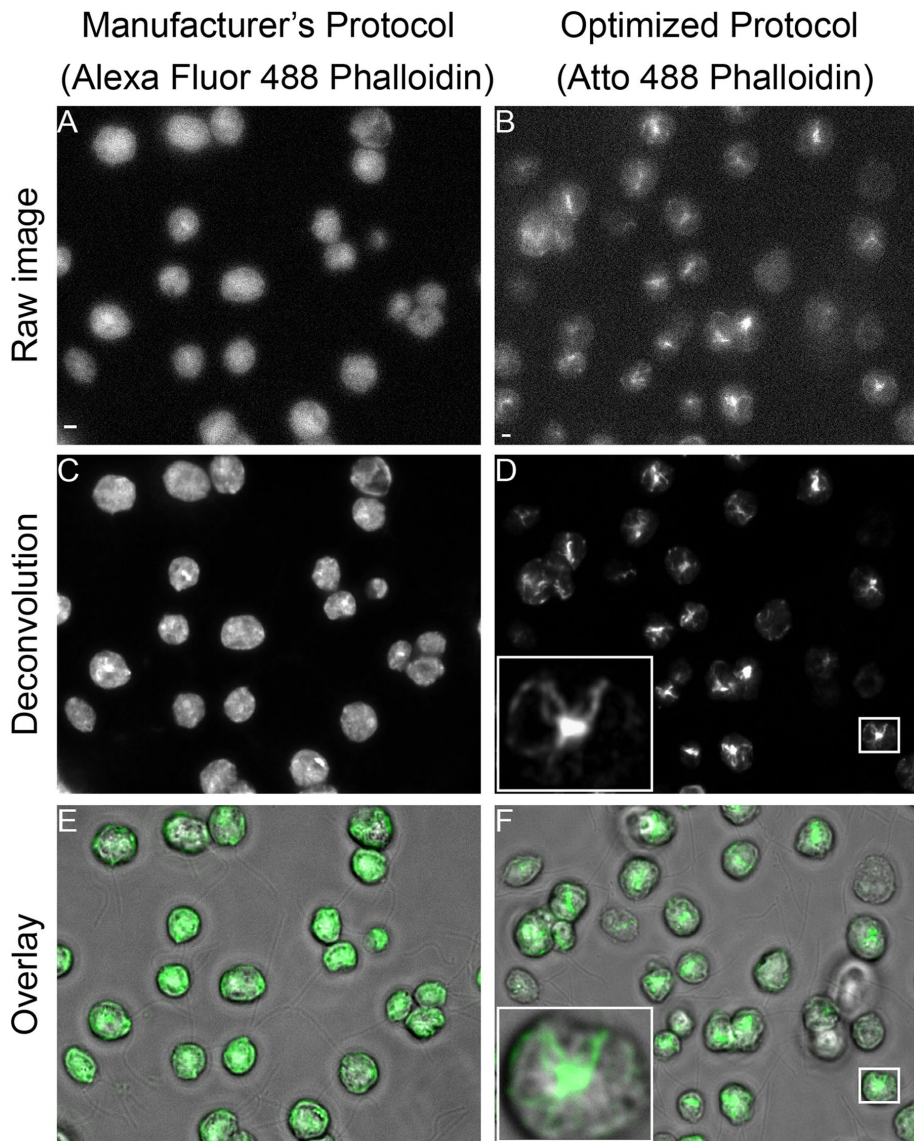


FIGURE 1: Filamentous actin staining optimization using phalloidin in *Chlamydomonas reinhardtii*. (A) Raw fluorescence image of phalloidin-stained vegetative *Chlamydomonas* cells using the manufacturer's recommended protocol and Alexa Fluor 488 phalloidin. Signal is generally bright with hazy fluorescence throughout the cell, similar to previous reports. (B) Raw fluorescence image using our optimized phalloidin protocol and Atto 488 phalloidin (49409; Sigma) reagent. Signal from filamentous actin is clearly present. (C) Deconvolution of the image in A does not reveal much actin signal that can be easily distinguished from the high background fluorescence. (D) Deconvolution of B shows filamentous actin posterior of the nucleus and filaments spanning across the cell body. (E) Overlay of C and the brightfield image with phalloidin signal in green. (F) Overlay of D and the brightfield image shows that in vegetative cells, the brightness and staining consistency were greatly enhanced by using the Atto 488 conjugate instead of Alexa Fluor 488. Scale bar is 5 μm .

filamentous actin foci at their apex. We observed that the foci persisted in CC-124, suggesting that this apical staining may mark the formation of the mating type minus actin structure (Figure 5E, inset), which is a small membrane protrusion (Misamore *et al.*, 2003).

During artificial induction of gametes, fertilization tubules form after the addition of papavarine and dibutyl cAMP in mating type plus cells. This actin-rich fusion organelle protrudes from the apex of the cell, the same location where we observed apical actin accumulation in uninduced gametes (Figure 5C, inset). During tubule induction, the midcell filamentous actin population disappeared (Figure 5C).

However, this loss of midcell actin was not seen in mating type minus CC-124 cells, which do not form tubules (Figure 5F). This led to the hypothesis that midcell filamentous actin rearranges to form the tubules. To test this hypothesis, gametes were induced in the presence of cycloheximide (Figure 5, G–I), a drug that blocks translation (Supplemental Figure 2) and thus the up-regulation of actin expression that occurs during induction (Ning *et al.*, 2013). Strikingly, treatment with cycloheximide did not prevent tubule formation, and the number of tubules formed in the presence of cycloheximide was comparable to the number of tubules formed under control conditions (Figure 5, G–I). This result indicates that fertilization tubules do not require newly synthesized actin and instead can be formed by the redistribution of existing actin to the cell apex.

Actin dynamics throughout the *Chlamydomonas* cell cycle

Previously, Harper *et al.* (1992) investigated total actin dynamics in *Chlamydomonas* using actin antibodies. With our newly established ability to specifically monitor the filamentous actin population, we synchronized cells using a light/dark regime to track filamentous actin through the cell cycle. The *Chlamydomonas* nucleus positioning and morphology, visualized by costaining with DAPI, acted as an indicator for cell cycle events. For interphase cells, which are recognizable by the nucleus's central position, Harper and colleagues (1992) reported diffuse actin localization surrounding the nucleus. Our data suggest actin filament localization is strictly perinuclear, and the Atto 488 phalloidin signal often revealed more linear structures compared with diffuse total actin staining (Figure 6A). Additionally, we see punctate apical actin signal in some cells, but we have not been able to observe a cell cycle-dependent pattern to these puncta. In preprophase, we observe that actin forms an angular shape around part of the nucleus (Figure 6B). In prophase, there is a dense epicenter of filamentous actin signal near the nucleus, but a few actin threads still remain that stretch across the cell (Figure 6A). Metaphase and anaphase are recognizable by the flattening of the DAPI signal, indicating that condensed chromosomes are aligning for segregation. During this stage of the cell cycle, filamentous actin creates a linear arrangement behind the nucleus (Figure 6C). We observe filamentous actin localization during early telophase, where filaments localize to both sides of the nucleus to help initiate cleavage furrow formation, similar to total actin dynamics seen by Harper *et al.* (1992) (Figure 6D). Previously, total actin was shown to return to its state of diffuse localization around the reformed daughter nuclei. We did not observe actin filaments completely surrounding nuclei, regardless of cell

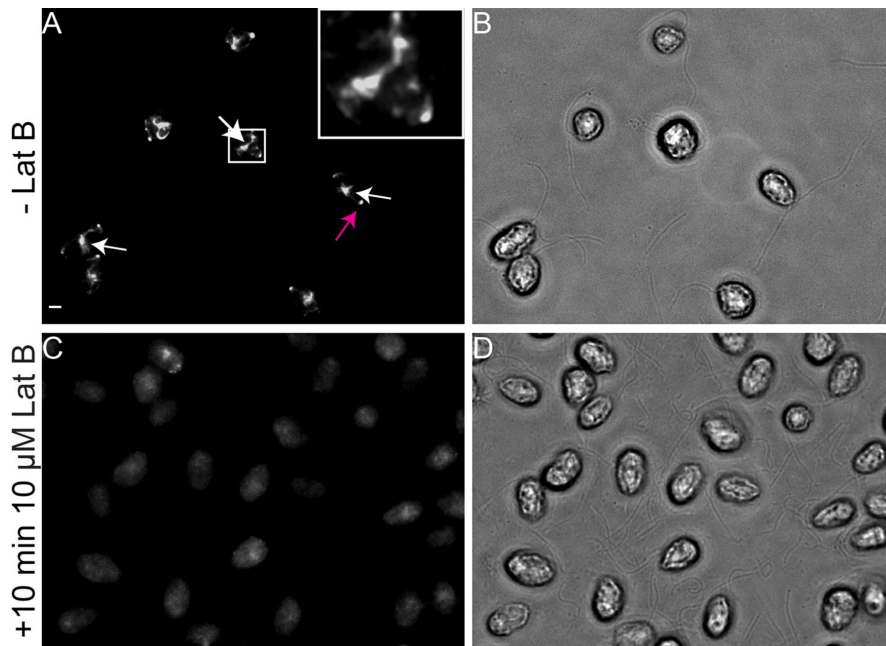


FIGURE 2: Phalloidin-labeled filamentous actin depolymerizes upon Lat B treatment in wild-type CC-125 cells. (A) Gametic CC-125 cells stained with Atto 488 phalloidin, showing midcell actin staining (white arrows) and apical actin fluorescence (magenta arrow). (B) Brightfield image of the cells in A showing filamentous actin signal. (C) Atto 488 phalloidin-stained gametic CC-125 cells after 10 min of treatment with 10 μ M Lat B. Filamentous actin signal dramatically decreases. (D) Brightfield image of cells in C show filamentous actin signal in relation to the cell body and flagella. Scale bar is 5 μ m.

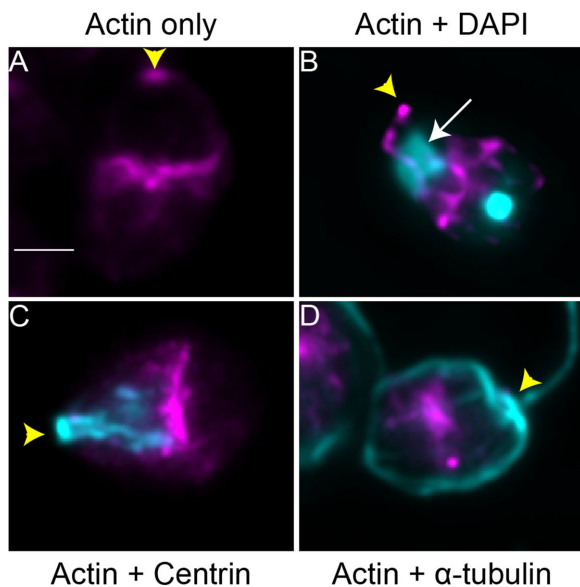


FIGURE 3: Actin colabeling with cellular structures. (A) Representative image of filamentous actin localization (magenta) in a *Chlamydomonas* cell stained with Atto 488 phalloidin. (B) Atto phalloidin and DAPI costaining, showing filamentous actin (magenta) in relation to the *Chlamydomonas* nucleus (cyan). The intense punctate DAPI staining toward the cell's basal side labels chloroplast DNA packed within DNA-protein structures called nucleoids. The nucleus is marked with an arrow and has broader and less intense DAPI staining. (C) Cell costained with phalloidin (magenta) and anti-centrin antibody (cyan). (D) Cell costained with phalloidin (magenta) and anti- α -tubulin antibody, which marks axonemal and cytoplasmic microtubules (cyan). Yellow arrowheads specify the apical end of the cell. Scale bar is 5 μ m.

cycle stage. This suggests that the diffuse population is exclusively monomeric. Cytokinetic actin filaments are present at the cleavage furrow (Figure 6E), consistent with the pattern previously seen with total actin staining. Throughout mitosis, a population of actin filaments can be seen near the cell cortex, which is typically not present in interphase cells.

Visualization of conventional and nonconventional actins

After localizing IDA5 filaments in gametic and cycling cells, we wondered whether NAP1 could form distinct structures. Treating wild-type cells with the actin-depolymerizing drug Lat B for 10 min eliminated the specific midcell filamentous actin staining (Figure 7B). Lat B incubation for longer times, which is known to up-regulate NAP1 expression (Onishi *et al.*, 2016), resulted in the formation of transient actin ring structures (Figure 7C). Costaining cells with phalloidin and DAPI after 45 min of Lat B treatment showed that filamentous actin rings assemble around the nucleus (Figure 7D and Supplemental Movies 1 and 2). The prevalence of these rings in the cell population peaked at 60 min and then decreased until 150 min, at which point the rings had almost completely disassembled (Figure 7F). Live-cell imaging using a LifeAct-Venus trans-

formant revealed a similar ring phenotype, often accompanied by an additional linear or dot-like signal rarely observed in phalloidin-stained cells (Figure 7E). Another difference between the LifeAct-Venus and phalloidin-stained cells is the onset of ring formation, as ring structures do not begin to form until around 2 h of Lat B treatment in LifeAct-Venus cells. The variable timing of ring onset may be due to the differences in strain background between the LifeAct-expressing strain and the CC-125 wild-type strain. Alternatively, LifeAct binding may interfere with ring formation in live cells due to its documented effects on altering endogenous actin networks (Courtemanche *et al.*, 2016; Flores *et al.*, 2019).

On the basis of the Lat B-induced up-regulation of NAP1 expression and the insensitivity of NAP1 to Lat B (Onishi *et al.*, 2016), we hypothesized that this ring structure is composed of NAP1 filaments. We first attempted to visualize the two *Chlamydomonas* actins independently by staining *nap1* mutants (expressing only IDA5) and *ida5* mutants (expressing only NAP1) with Atto 488 phalloidin. Atto 488 phalloidin staining in *nap1* vegetative cells displayed a wild-type-like midcell actin signal (Figure 8, A and C), and a single apical spot was often present (Figure 8C). However, in *ida5* mutants, the signal remained weak and hazy (Figure 8E). This may be due to low NAP1 abundance or slight sequence differences in the phalloidin binding sites of IDA5 and NAP1. Actin has two methionine residues that are critical for phalloidin binding, which are conserved in the IDA5 sequence. However, NAP1 contains mutations at both methionine sites, which could reduce phalloidin's ability to label NAP1 filaments (Vandekerckhove *et al.*, 1985).

Despite poor efficiency of labeling low endogenous levels of NAP1, we reasoned that increases in NAP1 expression upon Lat B treatment (Onishi *et al.*, 2018) and increased local filament concentration may still allow for phalloidin-labeling of rings composed of

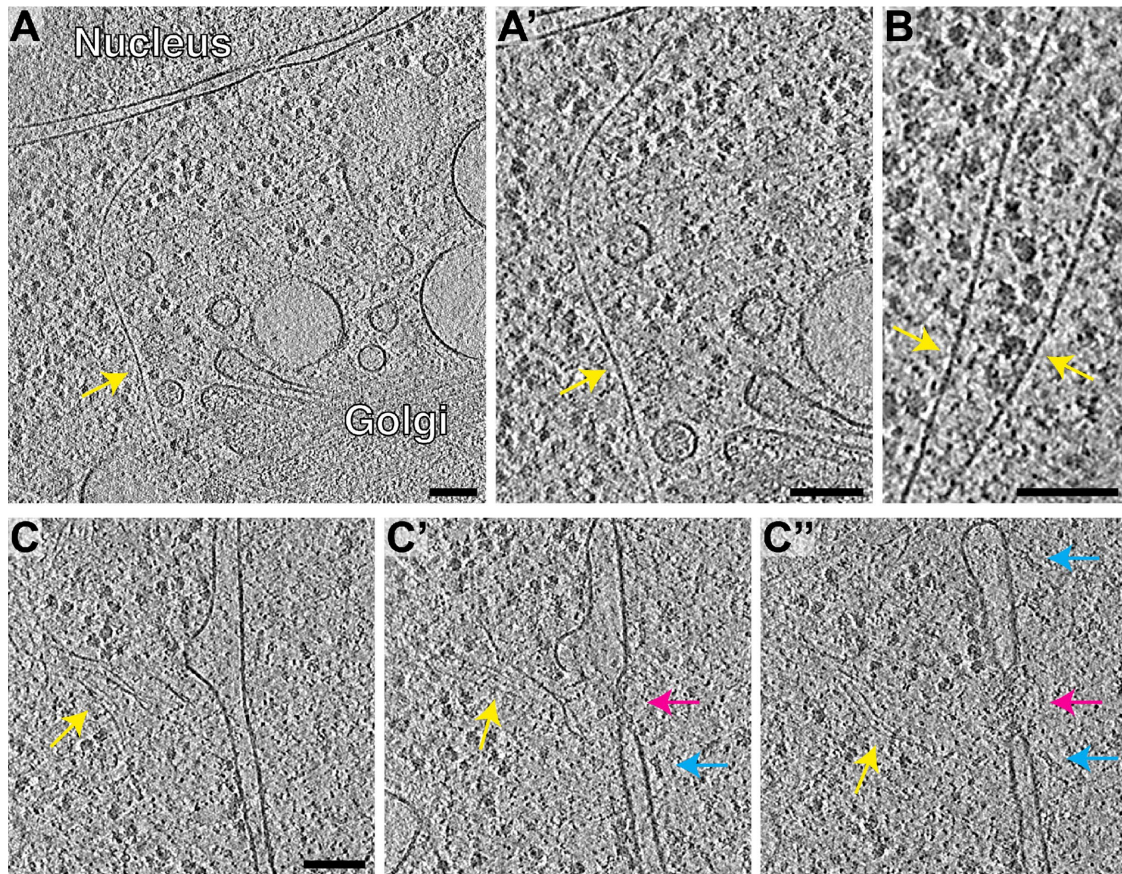


FIGURE 4: Direct visualization of actin filaments inside native *Chlamydomonas* cells by in situ cryo-ET. (A, B) Slices through tomographic volumes. Yellow arrows indicate individual actin filaments near the nuclear envelope and Golgi apparatus. A' is an enlarged view of the filament from A. The helical structure of the actin filaments is apparent in B. (C) A loose bundle of actin filaments (yellow arrow) in close proximity to a nuclear pore complex (magenta arrow). Clearly resolved nuclear proteasomes tethered to the nuclear pore complex (blue arrows, previously described in Albert *et al.*, 2017) illustrate the molecular clarity of this tomogram. C, C', and C'' show three different slices through one tomographic volume. Scale bars are 100 nm in all panels.

NAP1. To test whether rings require NAP1, we treated the *nap1* mutant with Lat B for 45 min. In the absence of drug, Atto 488 phalloidin-stained *nap1* cells displayed similar wild-type-like midcell actin signal (Figure 8C). However, Lat B treatment did not result in the formation of filamentous ring structures in *nap1* cells (Figure 8D), suggesting that ring assembly is NAP1-dependent. Furthermore, Lat B-treated *ida5* cells that express only NAP1 are capable of forming these ring structures, albeit at a much lower frequency (Figure 8F). These results demonstrate that NAP1 is necessary and sufficient for ring formation.

DISCUSSION

The coordinated expression and polymerization of two actins that share ~65% sequence identity within the same cell can provide broader insight into mechanisms of actin regulation and segregation of actin-dependent functions in vivo. The two *Chlamydomonas* actin genes are poorly characterized. One reason for this is that the *ida5* null mutant appears to have a mild, wild-type-like phenotype. We now believe this is due to compensation by the up-regulation of NAP1 in *ida5* mutants (Kato-Minoura, 2005; Onishi *et al.*, 2016, 2018). Loss of both actins is lethal (Onishi *et al.*, 2016), and our recent studies demonstrate partially redundant functions for the two actins at multiple stages of ciliary assembly (Jack *et al.*, 2019).

Outside of the compensatory functions, the requirement for dual expression is not clear because NAP1 expression is undetectable under normal conditions and only up-regulated slightly in the absence of IDA5 or strongly upon flagellar reassembly following deflagellation (Hirono *et al.*, 2003). Despite the up-regulation of NAP1 upon flagellar regeneration, we previously found that *nap1* null mutants have no flagellar assembly defect outside of the inability to buffer perturbations to IDA5 (Jack *et al.*, 2019). NAP1 can largely perform the functions of filamentous IDA5, as *ida5* mutants show only slow swimming. This is likely due to the loss of four axonemal inner dynein arm subspecies within flagella (Kato-Minoura *et al.*, 1997) and slow initial phases of flagellar assembly (Avasthi *et al.*, 2014). NAP1 cannot replace IDA5 in all cases, however. Despite localization of NAP1 to actin-rich fertilization tubules (Hirono *et al.*, 2003), *nap1* mutant cells assemble normal fertilization tubules (Christensen *et al.*, 2019) and *ida5* mutants expressing NAP1 alone form structurally defective fertilization tubules, resulting in a drastically reduced mating efficiency (Kato-Minoura *et al.*, 1997).

To complement our functional studies of IDA5 and NAP1, we wanted to understand whether the two proteins exhibit similar localization and dynamics. However, actins in *Chlamydomonas* have been difficult to visualize by fluorescence microscopy and traditional electron microscopy. Actin mutant phenotypes suggest

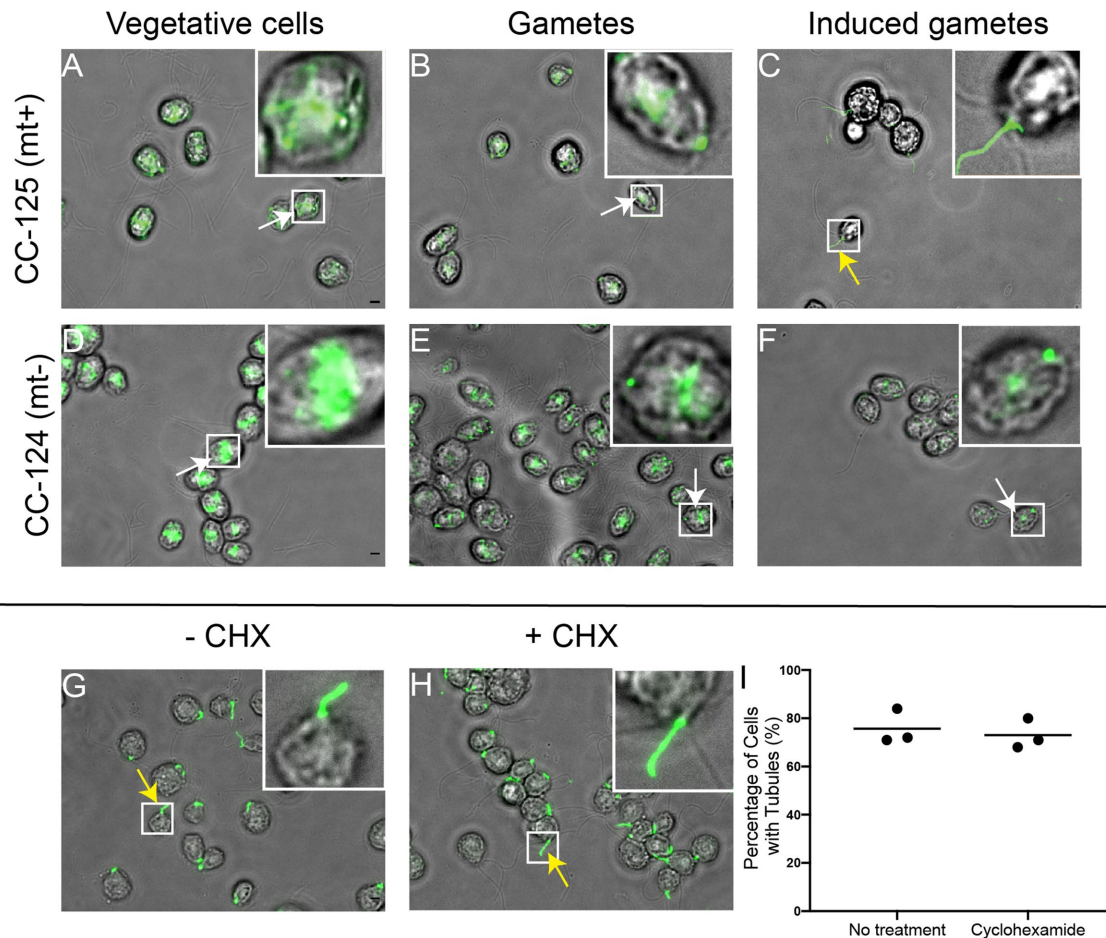


FIGURE 5: Expression-independent reorganization of actin filaments during gamete induction. All cells stained with Atto 488 phalloidin. Actin in green. (A) Vegetative CC-125 cells of the mating type plus background show perinuclear actin signal. (B) Gametic CC-125 cells often display a single apical actin pool near the site of eventual fertilization tubule formation. (C) Inducing gametic CC-125 cells with papavarine and dibutyryl cAMP causes cells to form actin-rich fertilization tubules. (D) Vegetative CC-124 cells of the mating type minus background have comparable actin signal to vegetative CC-125. (E) Gametic CC-124 also show frequent apical actin signal. (F) Induced CC-124 cells retain the midcell actin population and do not form long fertilization tubules observed in CC-125 cells, but a small actin pool does accumulate near the apical surface in these cells. (G) CC-125 cells induced under control conditions form fertilization tubules. (H) CC-125 cells induced in the presence of 10 μ M cycloheximide still form a comparable number of fertilization tubules, suggesting that the increased actin expression caused by gametic induction is not required for tubule formation. Scale bars are 5 μ m. (I) Quantification of the percentage of cells that form fertilization tubules in the presence of 10 μ M cycloheximide. Dots represent means from three separate experiments where $n = 100$ cells in each experiment. The mean of these three experiments is represented by a line.

actin localization in flagella, fertilization tubules, and the cleavage furrow. Indeed, this has been visualized using phalloidin in fertilization tubules (Wilson *et al.*, 1997) and actin antibodies (which cannot discriminate between actin monomers and filaments) in the cleavage furrow (Ehler and Dutcher 1998; Kato-Minoura *et al.*, 1998). It was reported that phalloidin did not clearly label filamentous structures in vegetative *Chlamydomonas* cells after 2 h of staining; instead, only bright fluorescence throughout the cell body could be observed (Harper *et al.*, 1992). Recently, it was shown that *Chlamydomonas* cells deficient in peptidylglycine α -amidating monooxygenase (PAM) displayed altered actin organization. PAM knockdown cells displayed patches of filamentous actin via bodipy-phalloidin staining, whereas control cells exhibited only diffuse cytoplasmic signal, a common result when using a non-*Chlamydomonas* optimized phalloidin protocol (Kumar *et al.*, 2018). We initially encountered similar results, even when using a

much shorter incubation time of 30 min. However, reducing the staining time to 16 min resulted in optimal signal to noise and clear labeling of filamentous structures. Despite this improvement, many phalloidin trials using this 16-min incubation time resulted in a bright and diffuse signal in the cell body, and cells were susceptible to rapid photobleaching during imaging. These inconsistencies were alleviated after switching to a different phalloidin conjugate, Atto 488 phalloidin, which produced a clear and consistent photostable signal (Supplemental Figure 1).

The addition of this reagent to our optimized actin staining protocol led to a powerful and reproducible method for visualizing filamentous actin in fixed vegetative *Chlamydomonas* cells (Craig and Avasthi, 2019). Combining three independent visualization methods (live-cell LifeAct labeling, fixed-cell phalloidin labeling, and direct imaging of filaments inside native cells by cryo-ET) with analysis of Lat B sensitivity, our study confirms that *Chlamydomonas*

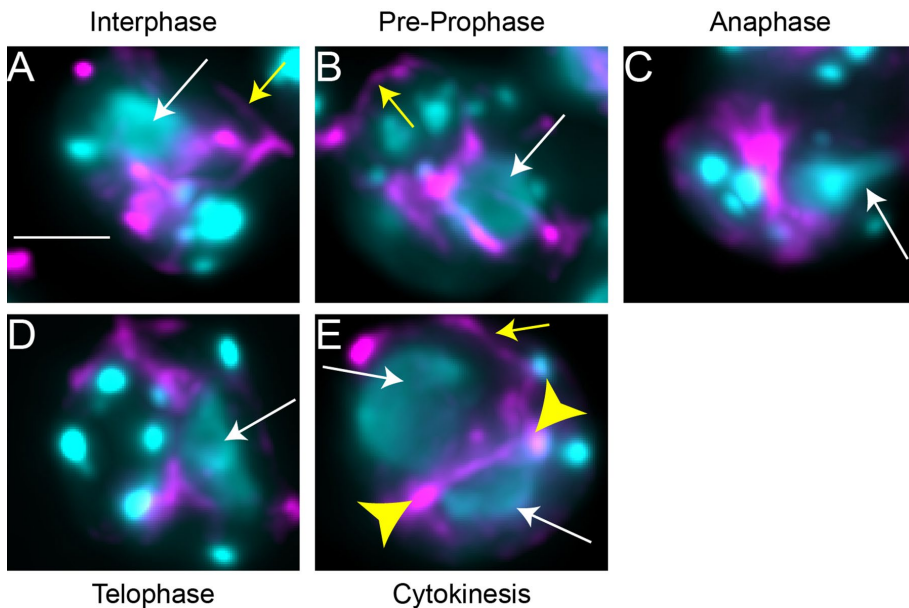


FIGURE 6: Filamentous actin localization across the cell cycle. Atto 488 phalloidin (magenta) and DAPI (cyan) costaining. The intense smaller DAPI puncta are chloroplast nucleoids. The nuclei (white arrows) have larger and less intense DAPI staining. (A) Filamentous actin is found posterior to the nucleus in interphase cells. (B) In early prophase, filamentous actin forms additional bands connecting the midcell actin to the apical side of the cell. (C) During anaphase, filamentous actin appears orthogonal to the elongating nucleus. (D) In early stages of telophase, filamentous actin pinches on both sides of the nucleus. (E) During cytokinesis, linear actin filaments are present in the cleavage furrow (yellow arrowheads). Throughout the mitotic stages, additional actin filaments appear around the cell cortex. Scale bar is 5 μ m.

cells have a bona fide actin filament network at the posterior of the nucleus that occasionally extends to the flagellar base at the apex of the cell (Figure 9).

Our study reveals previously unreported filamentous structures in *Chlamydomonas*. Most obvious is the array of filamentous actin localized posterior of the nucleus in vegetative and gametic cell types. The actin-binding and nucleating proteins responsible for coordinating this actin population are not known, but recent findings in our lab strongly suggest a role for actin in trafficking vesicles from the Golgi (Jack *et al.*, 2019). This midcell actin revealed by Atto phalloidin along with cryo-ET showing distinct actin filaments near the Golgi (Figure 4A) steers us to investigate the functional role of actin in ciliary protein transport (Avasthi *et al.*, 2014; Jack *et al.*, 2019). The midcell actin is likely composed of IDA5 filaments, as we see similar actin localization when labeling *nap1* mutant cells and no filamentous signal in this region when labeling *ida5* mutants. NAP1 expression is undetectable in unperturbed vegetative cells, but increased in *ida5* mutant cells (Ohara *et al.*, 1998) and additionally increased to a small degree in Lat B-treated *ida5* mutants (Onishi *et al.*, 2018). This increased expression and concentration of NAP1 may contribute to the ability to visualize infrequent rings in Lat B-treated *ida5* mutants. Although we have struggled to visualize the normal population of filamentous NAP1 with phalloidin staining, we are pursuing improved stability LifeAct probes and alternative strategies.

We provide the first report of filamentous actin dynamics across the *Chlamydomonas* cell cycle, and find several new labeling patterns compared with the total actin localization initially reported by Harper *et al.* (1992). Filamentous actin is dynamic throughout the cell cycle and redistributes most dramatically in telophase and cytokinesis (Figure 6, D and E). Total actin staining shows diffuse

localization around the entire nucleus, whereas filamentous actin remains strictly linear and posterior to the nucleus until early telophase. Although filaments can be seen in the cleavage furrow in telophase and between the two daughter nuclei during cytokinesis, no ring structure is seen during ingression. *Chlamydomonas* cells instead use a microtubule-dependent structure called the phycoplast for cytokinesis (Johnson and Porter, 1968; Holmes and Dutcher, 1989; Gaffal and el-Gammel, 1990; Schibler and Huang, 1991). Our data show that mitotic cells also appear to have additional actin filaments near the cell cortex (Figure 6, A, B, and E). As *Chlamydomonas* cells divide several times before breaking out of the mother cell wall, the cell wall is not immediately adjacent to the plasma membrane of daughter cells during division. Actin filaments adjacent to the cortex may provide structural support during this stage. Further characterizing this filament population and observing the effects of actin inhibitors on daughter cell morphology will help determine the role of these filaments.

We consistently observed apical accumulation of filamentous actin between the flagella in gametic cells, and more variable apical signal in vegetative cells. We believe this filamentous actin population in gametes

serves as an actin recruitment site, perhaps supplying a pool of actin monomers for building the highly filamentous fertilization tubule formed in mating type plus gametic cells. It is thought that fertilization tubules may assemble from newly synthesized actin, as actin expression is known to increase during gamete activation and mating (Hirono *et al.*, 2003). However, treatment with cycloheximide to block transcription during induction did not significantly reduce the percentage of cells that formed fertilization tubules (Figure 5I). Thus, tubule formation can occur without increased expression, suggesting that there is a common pool of monomers that can either form the network of midcell actin filaments or remodel to form other actin structures like fertilization tubules. This implies that the fertilization tubule serves as a sink for monomers that causes the concentration of the monomers in the middle of the cell to drop below the critical concentration for polymerization, resulting in the loss of the midcell actin filaments. This hypothesis is further supported by our observation that induction of mating type minus cells, where fertilization tubules do not form, does not result in a loss of filamentous actin.

We rarely observed actin mislocalization from the subflagellar region or multiple spots of apical accumulation in gametes. A well-conserved function of actin is in endocytosis. It is possible that the variable spots we see at the cell periphery in vegetative cells are analogous to endocytic patches or pits. Although there is little evidence for endocytosis in *Chlamydomonas*, studies of cell adhesion during mating show that activity-dependent redistribution of signaling proteins from the cell body plasma membrane into cilia seems to occur in a microtubule-dependent manner but is independent of ciliary motors (Belzile *et al.*, 2013). This leaves open the possibility that the redistribution of the membrane proteins may involve actin-dependent endocytosis and intracellular trafficking using cytoplasmic microtubule motors.

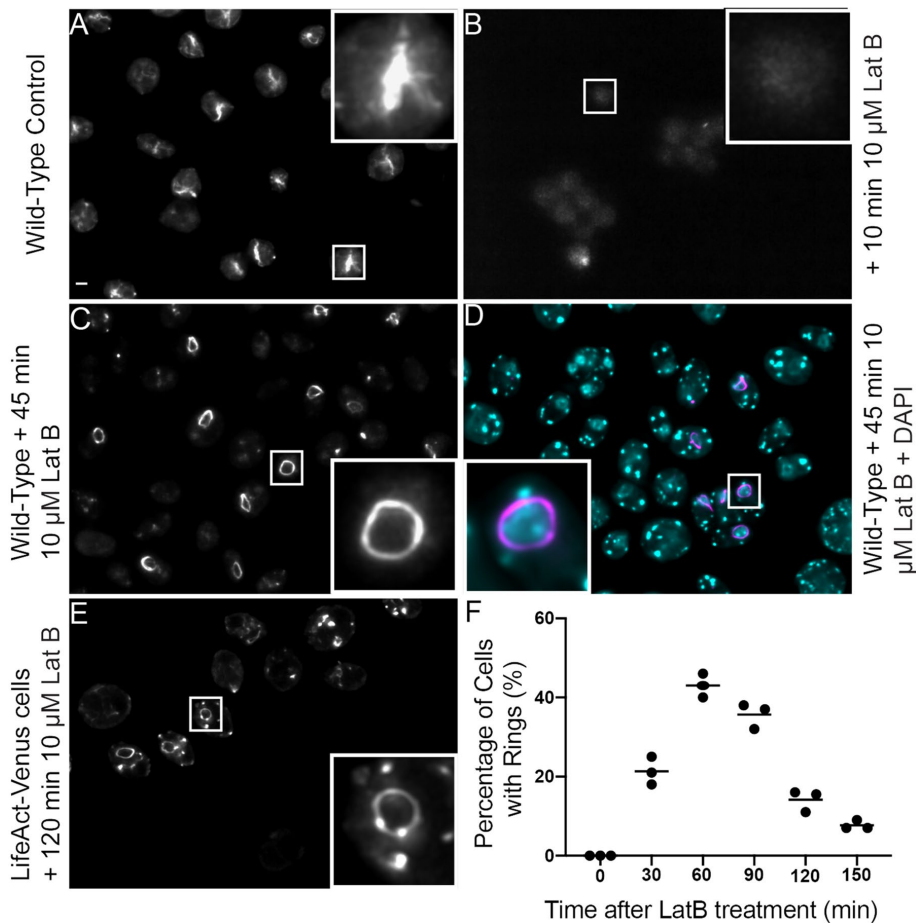


FIGURE 7: Ring-like actin structures in CC-125 cells are induced by prolonged Lat B treatment. (A) Vegetative wild-type CC-125 cells stained with Atto 488 phalloidin. (B) The filamentous actin signal disappears after 10 min of treatment with 10 μ M Lat B. Cells stained with Atto 488 phalloidin. (C) Filamentous actin ring structures form in many CC-125 cells after 45 min of treatment with 10 μ M Lat B. Cells stained with Atto 488 phalloidin. (D) Actin ring structures colocalize around the nucleus under identical treatment conditions in wild-type cells. Actin in magenta; DAPI in cyan. (E) Live LifeAct–Venus cells treated with 10 μ M Lat B for 120 min also show the actin ring phenotype. Scale bar is 5 μ m. (F) Bar graph depicting ring frequency in populations of Lat B–treated wild-type cells stained with Atto 488 phalloidin. Dots represent means from three separate experiments where $n = 200$ cells in each experiment. The mean of these three experiments is represented by a line.

We found that NAP1 is both necessary and sufficient for formation of phalloidin-stained perinuclear rings induced by Lat B. However, given the low frequency of ring formation in *ida5* mutant cells, we cannot rule out the possibility that the Lat B rings in wild-type cells are made of IDA5/NAP1 copolymers. These ring structures appeared after ~ 30 min of Lat B treatment, became most frequent at 1 h, and dissipated by 2 h (Figure 7F). This timing is consistent with findings from Onishi *et al.* (2016) and Onishi *et al.* (2018), where Lat B–induced NAP1 expression was measured by RT-PCR, RNAseq, and Western blot. NAP1 expression levels dramatically increased at 30 min after the addition of 10 μ M Lat B. Although the onset of ring formation is coincident with an up-regulation of actin, ring frequency declines while levels of actin expression remain elevated. Given the transient nature of the actin rings, it is possible that these rings acutely compensate for actin-dependent functions to protect the nucleus. These functions may include regulating nuclear shape (Khatau *et al.*, 2009), nuclear positioning (Gundersen

and Worman, 2013), or connecting with the nucleoskeleton to transduce mechanical signals (Tapley and Starr, 2013). The ring may interact with nuclear pore complexes (Moslaganti *et al.*, 2018), as we observed a cluster of filaments gather near one of these sites before Lat B disruption (Figure 4C). Another possibility is that ring formation may be involved in nuclear rupture (Hatch and Hetzer, 2016; Wesolowska *et al.*, 2018). Although actin-dependent nuclear envelope rupture does not kill cells in all circumstances, a decrease in frequency of rings at the population level after 2 h may be due to the death of ring-containing cells. Live-cell microscopy following individual cells or analysis of synchronized populations will likely discriminate between these possibilities.

A seemingly universal function of actin is directing mitotic and meiotic events by localizing vesicles and the cytokinetic machinery in plant, fungi, and animal cells. Filamentous actin-rich ring structures have been associated with cytokinesis in animal cells (Wang, 2005) and yeast (Arai and Mabuchi, 2002). Many of these rings undergo a constriction that is mediated by a contractile class II myosin. Given that *Chlamydomonas* cells lack this type of myosin, we believe the NAP1-dependent ring structures are unlikely to be an analogue to contractile actin rings used for cell division.

The coexpression of a conventional and divergent actin within a single cell establishes *Chlamydomonas* as an excellent new system to identify fundamental principles of actin biology. Robust visualization of the filamentous actin network in these cells may reveal novel modes of actin-dependent regulation for major cellular processes, such as ciliary biology and photosynthesis, for which *Chlamydomonas* is already a leading model organism.

MATERIALS AND METHODS

Chlamydomonas strains

The wild-type strains CC-125 mt +, CC-124 mt –, and *mat3-4* strain CC-3994 mt + were obtained from the Chlamydomonas Resource Center (University of Minnesota). The *nap1* mutant was a generous gift from Fred Cross (The Rockefeller University), Masayuki Onishi (Stanford University), and John Pringle (Stanford University). The LifeAct–Venus wild-type transformant was gifted by Masayuki Onishi, Stanford University.

Phalloidin staining

Cells were grown in 2 ml of TAP (Tris acetate phosphate) liquid media on a roller drum for 17 h (overnight). It is essential to select healthy cells by centrifuging 1 ml of cell culture at 1800 rpm for 1.5 min. The supernatant was discarded and cells were resuspended in 600 μ l fresh TAP. Resuspended cells (200 μ l) were adhered on poly-L-lysine–coated coverslips for 5 min and covered. The liquid was tilted off the

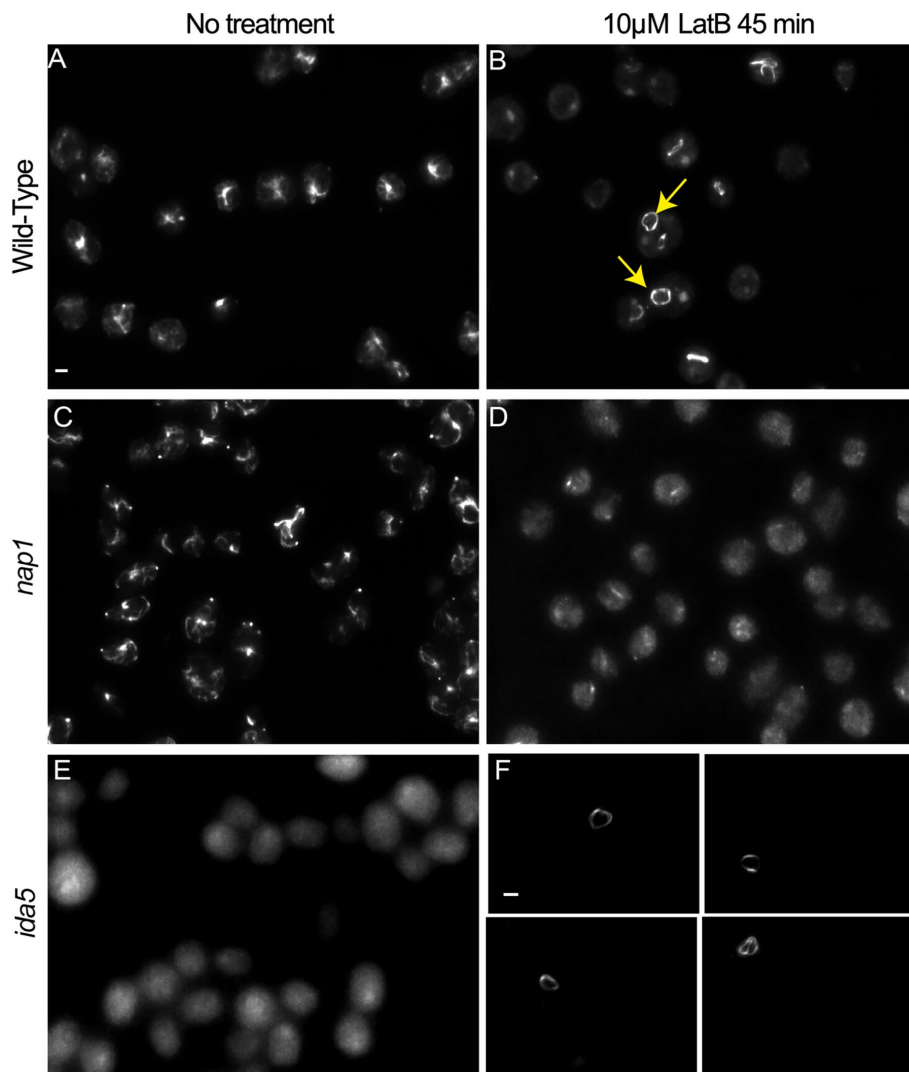


FIGURE 8: NAP1 is necessary and sufficient for assembly of the ring-like filamentous structure in Lat B-treated cells. (A) Vegetative wild-type CC-125 cells stained with Atto 488 phalloidin. (B) Lat B-treated wild-type cells displaying actin rings. (C) Vegetative *nap1* cells stained with Atto 488 phalloidin display similar actin signal to wild-type cells. (D) Rings do not form in *nap1* cells treated with 10 μ M Lat B for 45 min. (E) Atto 488 phalloidin labeling does not detect filaments in *ida5* stained cells. (F) Very few (<3%) *ida5* cells form actin rings under Lat B treatment conditions. Scale bars are 5 μ m.

coverslips and replaced with 4% fresh paraformaldehyde (PFA) in 7.5 mM HEPES, pH 7.24. The PFA is prepared from a 16% fresh ampoule of PFA. See Farhat (2013) for a detailed protocol for making this fixative solution. The pattern of staining changes (producing a bright pyrenoid signal) and nonspecific cytoplasmic fluorescence increases if using PFA that is not fresh. Coverslips were washed with 1X phosphate-buffered saline (PBS) for 3 min. For cell permeabilization, coverslips were submerged in a coplin jar containing 80% precooled acetone and then incubated for 5 min at -20°C . Coverslips were quickly transferred to a second coplin jar containing 100% precooled acetone and incubated again for 5 min at -20°C . Coverslips were allowed to air dry for a minimum of 2 min, and for longer if needed. Next, cells were rehydrated by transferring coverslips to a coplin jar containing 1X PBS for 5 min. Coverslips were then stained with Atto 488 phalloidin (49409; Sigma) for 16 min in the dark, significantly reducing background and increasing the signal-to-noise ratio. The Atto 488 phalloidin reagent greatly enhanced photostability and brightness

compared with Alexa Fluor 488 phalloidin (Supplemental Figure 1), which allowed for more uniform and reproducible filament labeling. Phalloidin incubation was followed by a wash in 1X PBS for 5 min. Finally, coverslips were mounted on slides as quickly as possible with self-sealing Fluoromount-G (Invitrogen). We have published a more detailed protocol (Craig and Avasthi, 2019).

Cell synchronization

For experiments requiring synchronous cultures, cells were grown in HS media (Sueoka, 1960) and followed a 14 h light, 10 h dark growth regime. To initiate the dark period, culture tubes were wrapped in tin foil to prevent light exposure. Cells were immediately fixed following transition to the dark period and stained according to the phalloidin protocol above. For nucleic acid labeling, 200 μ l of 1:3000 10 mg/ml DAPI solution in 1X PBS was added to the phalloidin staining solution for the final 10 min of phalloidin incubation. Cell cycle events were identified by nuclear morphology and localization in light-dark synchronized cultures.

Immunofluorescence for colocalization microscopy

Wild-type cells were grown overnight in TAP media. Cells were treated following the general phalloidin staining protocol up to the rehydration step. After cells had been rehydrated in 1X PBS for 5 min, cells were incubated in 100% block solution (5% bovine serum albumin, 1% cold water fish gelatin in 1X PBS) for 30 min, followed by a secondary blocking step containing 10% normal goat serum in block solution for another 30 min. Cells were incubated in either 1:500 anti-centrin or 1:500 anti- α -tubulin overnight in a humidified chamber. The next morning, cells were washed three times (10 min each) with 1X PBS. Cells were stained with anti-mouse594 diluted 1:500 for 1 h, and stained

with Atto 488 phalloidin for the final 16 min of the stain. Cells were then washed three times (10 min each) in 1X PBS, mounted on slides with Fluoromount-G, and imaged on a Nikon TiS microscope.

Cell vitrification and FIB milling

Chlamydomonas cells were grown and prepared for cryo-ET as previously described (Albert et al., 2017; Bykov et al., 2017). We used the *mat3-4* strain (Umen and Goodenough, 2001), which has smaller cells that improve vitrification by plunge-freezing. Cells were grown with constant light (~ 90 $\mu\text{mol photons m}^{-2} \text{s}^{-1}$) in TAP medium, bubbling with normal air. Liquid culture (5 μ l, ~ 1000 cells/ μ l) was blotted onto carbon-coated 200-mesh copper grids (Quantifoil Micro Tools), which were then plunged into a liquid ethane-propane mixture using a Vitrobot Mark 4 (FEI Thermo Fisher). Frozen grids were mounted into modified autogrids (FEI Thermo Fisher) and loaded into either a Scios (FEI Thermo Fisher) or a Quanta 3D FEG (FEI Thermo Fisher) FIB/SEM microscope.

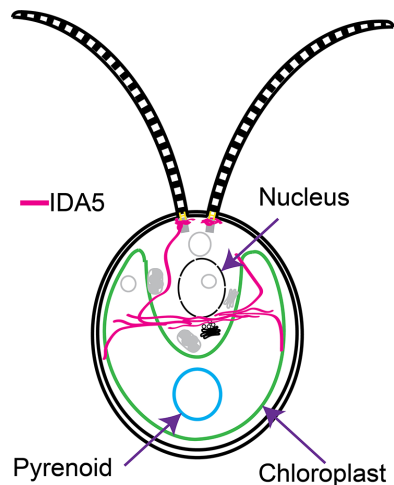


FIGURE 9: Distribution of filamentous actin in *Chlamydomonas*. Diagram depicting IDA5 filaments (pink) relative to landmark *Chlamydomonas* organelles. Actin filaments are predominantly localized basal of the nucleus, near the Golgi, but strands also extend throughout the cell to locations including the flagellar base.

The grids were coated with a thin layer of organometallic platinum using the gas injection system (FEI Thermo Fisher), and then the Ga⁺ beam was used to mill thin lamellae (100–200 nm thick), following the protocols detailed in Schaffer et al. (2015, 2017).

Cryo-electron tomography

Tomography was performed on a 300 kV Titan Krios (FEI Thermo Fisher) equipped with a quantum postcolumn energy filter (Gatan) and a K2 Summit direct electron detector (Gatan) operated in movie mode at 12 frames per second. Using SerialEM software (Mastrorade, 2005), tilt series were acquired over an angular range of approximately -60° to $+60^\circ$, using a bidirectional tilt scheme with 2° increments. Cumulative electron dose was $\sim 100 \text{ e}^-/\text{\AA}^2$, the object pixel size was 3.42 Å, and defocus ranged from -4 to $-6 \mu\text{m}$. Raw image frames were aligned with MotionCorr2 software (Zheng et al., 2017), and tomograms were reconstructed in IMOD software (Kremer et al., 1996) using patch tracking and back projection. The images displayed in this article were binned twice. To enhance the contrast, we used the tom_deconv deconvolution filter (https://github.com/dtegunov/tom_deconv).

Fertilization tubule induction

To induce gametogenesis, cells were grown in M-N (M1 minimal media without nitrogen) overnight under growth lighting. Gametes were mixed with dibutyl cAMP (13.5 mM) and papaverine (135 μM) for 45 min to induce fertilization tubule formation (modified from Wilson et al., 1997). Cells were then stained in accordance with our phalloidin protocol (see above).

Lat B treatment

Lat B was purchased from Sigma and used with the specified concentrations and incubation times. Typically, depolymerizing treatment was performed for 10 min, and cells were treated for 45 min to induce NAP1 up-regulation and ring formation.

ACKNOWLEDGMENTS

We thank Masayuki Onishi, John Pringle, and Fred Cross for providing the *nap1* mutant. Thank you to members of the Avasthi lab for troubleshooting and manuscript feedback. We acknowledge

Wolfgang Baumeister and Jurgen Plitzko for enabling the cryo-ET work by providing support and instrumentation. This work was funded through National Institutes of Health grants P20GM104936 and P20GM103418 (to P.A.), Deutsche Forschungsgemeinschaft Grant no. EN 1194/1-1 as part of research unit FOR2092 (to B.D.E.), and The Max Planck Society.

REFERENCES

- Albert S, Schaffer M, Beck F, Mosalaganti S, Asano S, Thomas HF, Plitzko JM, Beck M, Baumeister W, Engel BD (2017). Proteasomes tether to two distinct sites at the nuclear pore complex. *Proc Natl Acad Sci USA* 114, 13726–13731.
- Arai R, Mabuchi I (2002). F-actin ring formation and the role of F-actin cables in the fission yeast *Schizosaccharomyces pombe*. *J Cell Sci* 115, 887–898.
- Asano S, Engel BD, Baumeister W (2016). *In situ* cryo-electron tomography: a post-reductionist approach to structural biology. *J Mol Biol* 428, 332–343.
- Avasthi P, Onishi M, Karpiak J, Yamamoto R, Mackinder L, Jonikas MC, Sale WS, Shoichet B, Pringle JR, Marshall WF (2014). Actin is required for IFT regulation in *Chlamydomonas reinhardtii*. *Curr Biol* 24, 2025–2032.
- Belzile O, Hernandez-Lara CI, Wang Q, Snell WJ (2013). Regulated membrane protein entry into flagella is facilitated by cytoplasmic microtubules and does not require IFT. *Curr Biol* 23, 1460–1465.
- Bykov YS, Schaffer M, Dodonova SO, Albert S, Plitzko JM, Baumeister W, Engel BD, Briggs JA (2017). The structure of the COPI coat determined within the cell. *eLife* 6, e32493.
- Christensen JR, Craig EW, Glista MJ, Mueller DM, Li Y, Sees JA, Huang S, Mets LJ, Kovar DR, Avasthi P (2019). *Chlamydomonas reinhardtii* formin FOR1 and profilin PRF1 are optimized for acute rapid actin filament assembly. *BioRxiv*, DOI: <https://doi.org/10.1101/096008>.
- Courtemanche N, Pollard TD, Chen Q (2016). Avoiding artefacts when counting polymerized actin in live cells with LifeAct fused to fluorescent proteins. *Nat Cell Biol* 18, 676–683.
- Craig E, Avasthi P (2019). Visualizing filamentous actin in *Chlamydomonas reinhardtii*. *Bio-Protoc* 9, e3274.
- Detmers PA, Carboni JM, Condeelis J (1985). Localization of actin in *Chlamydomonas* using antiactin and NBD-phalloidin. *Cell Motil* 5, 415–430.
- Dobrowolski JM, Niesman IR, Sibley LD (1997). Actin in the parasite *Toxoplasma gondii* is encoded by a single copy gene, ACT1 and exists primarily in a globular form. *Cell Motil Cytoskeleton* 37, 253–262.
- Ehler LL, Dutcher SK (1998). Pharmacological and genetic evidence for a role of rootlet and phycoplast microtubules in the positioning and assembly of cleavage furrows in *Chlamydomonas reinhardtii*. *Cell Motil* 40, 193–207.
- Farhat Y (2013). Reagent Preparation: HEPES Stock Solution (0.1 M, pH 7.4). *Protocol Place*. Dec 2013. <http://protocol-place.com>.
- Flores LR, Keeling MC, Zhang X, Sliogeryte K, Gavara N (2019). Lifeact-GFP alters F-actin organization, cellular morphology, and biophysical behavior. *Sci Rep* 9, 3241.
- Gaffal KP, el-Gammal S (1990). Elucidation of the enigma of the “metaphase band” of *Chlamydomonas reinhardtii*. *Protoplasma* 156, 139–148.
- Gundersen GG, Worman HJ (2013). Nuclear positioning. *Cell* 152, 1376–1389.
- Harper JD, McCurdy DW, Sanders MA, Salisbury JL, John PC (1992). Actin dynamics during the cell cycle in *Chlamydomonas reinhardtii*. *Cell Motil Cytoskeleton* 22, 117–126.
- Hatch EM, Hetzer MW (2016). Nuclear envelope rupture is induced by actin-based nucleus confinement. *J Cell Biol* 215, 27–36.
- Hirono M, Uryu S, Ohara A, Kato-Minoura T, Kamiya R (2003). Expression of conventional and unconventional actins in *Chlamydomonas reinhardtii* upon deflagellation and sexual adhesion. *Eukaryotic Cell* 2, 486–493.
- Holmes JA, Dutcher SK (1989). Cellular asymmetry in *Chlamydomonas reinhardtii*. *J Cell Sci* 94(Pt 2), 273–285.
- Jack B, Mueller DM, Fee AC, Tetlow AL, Avasthi P (2019). Partially redundant actin genes in *Chlamydomonas* control transition zone organization and flagellum-directed traffic. *Cell Rep* 27, 2459–2467.e3.
- Johnson UG, Porter KR (1968). Fine structure of cell division in *Chlamydomonas reinhardtii*. *J Cell Biol* 38, 403–425.
- Kato-Minoura T (2005). Impaired flagellar regeneration due to uncoordinated expression of two divergent actin genes in *Chlamydomonas*. *Zool J Linn Soc* 167, 571–577.
- Kato-Minoura T, Hirono M, Kamiya R (1997). *Chlamydomonas* inner-arm dynein mutant, *ida5*, has a mutation in an actin-encoding gene. *J Cell Biol* 137, 649–656.

- Kato-Minoura T, Uryu S, Hirono M, Kamiya R (1998). Highly divergent actin expressed in a *Chlamydomonas* mutant lacking the conventional actin gene. *Biochem Biophys Res Commun* 251, 71–76.
- Khatau SB, Hale CM, Stewart-Hutchinson PJ, Patel MS, Stewart CL, Searson PC, Hodzic D, Wirtz D (2009). A perinuclear actin cap regulates nuclear shape. *Proc Natl Acad Sci USA* 106, 19017–19022.
- Kilmartin JV, Adams AE (1984). Structural rearrangements of tubulin and actin during the cell cycle of the yeast *Saccharomyces*. *J Cell Biol* 98, 922–933.
- Kremer JR, Mastrorade DN, McIntosh JR (1996). Computer visualization of three-dimensional image data using IMOD. *J Struct Biol* 116, 71–76.
- Kumar D, Thomason, RT, Yankova M, Gitlin JD, Mains RE, Eipper BA, King SM (2018). Microvillar and ciliary defects in zebrafish lacking an actin-binding bioactive peptide amidating enzyme. *Sci Rep* 8, 4547.
- Mastrorade DN (2005). Automated electron microscope tomography using robust prediction of specimen movements. *J Struct Biol* 152, 36–51.
- Miraldi ER, Thomas PJ, Romberg L (2008). Allosteric models for cooperative polymerization of linear polymers. *Biophys J* 95, 2470–2486.
- Misamore MJ, Gupta S, Snell WJ (2003). The *Chlamydomonas* Fus1 protein is present on the mating type plus fusion organelle and required for a critical membrane adhesion event during fusion with minus gametes. *Mol Biol Cell* 14, 2530–2542.
- Mosalaganti S, Kosinski J, Albert S, Schaffer M, Strenkert D, Salomé PA, Merchant SS, Plitzko JM, Baumeister W, Engel BD, Beck M (2018). *In situ* architecture of the algal nuclear pore complex. *Nat Commun* 9, 2361.
- Ning J, Otto TD, Pfander C, Schwach F, Brochet M, Bushell E, Goulding D, Sanders M, Lefebvre PA, Pei J, et al. (2013). Comparative genomics in *Chlamydomonas* and *Plasmodium* identifies an ancient nuclear envelope protein family essential for sexual reproduction in protists, fungi, plants, and vertebrates. *Genes Dev* 27, 1198–1215.
- Ohara A, Kato-Minoura T, Kamiya R, Hirono M (1998). Recovery of flagellar inner-arm dynein and the fertilization tubule in *Chlamydomonas ida5* mutant by transformation with actin genes. *Cell Struct Funct* 23, 273–281.
- Onishi M, Pecani K, Jones T, Pringle JR, Cross FR (2018). F-actin homeostasis through transcriptional regulation and proteasome-mediated proteolysis. *Proc Natl Acad Sci USA* 115, E6487–E6496.
- Onishi M, Pringle JR, Cross FR (2016). Evidence that an unconventional actin can provide essential F-actin function and that a surveillance system monitors F-actin integrity in *Chlamydomonas*. *Genetics* 202, 977–996.
- Periz J, Whitelaw J, Harding C, Gras S, Del Rosario Minina MI, Latorre-Barragan F, Lemgruber L, Reimer MA, Insall R, Heaslip A, Meissner M (2017). *Toxoplasma gondii* F-actin forms an extensive filamentous network required for material exchange and parasite maturation. *eLife* 6, e24119.
- Perrin BJ, Ervasti JM (2010). The actin gene family: function follows isoform. *Cytoskeleton* 67, 630–634.
- Pollard TD, Blanchoin L, Mullins RD (2000). Molecular mechanisms controlling actin filament dynamics in nonmuscle cells. *Annu Rev Biophys Biomol Struct* 29, 545–576.
- Schaffer M, Engel B, Laugks T, Mahamid J, Plitzko J, Baumeister W (2015). Cryo-focused ion beam sample preparation for imaging vitreous cells by cryo-electron tomography. *Bio-Protoc* 5, e1575.
- Schaffer M, Mahamid J, Engel BD, Laugks T, Baumeister W, Plitzko JM (2017). Optimized cryo-focused ion beam sample preparation aimed at *in situ* structural studies of membrane proteins. *J Struct Biol* 197, 73–82.
- Schibler MJ, Huang B (1991). The colR4 and colR15 β -tubulin mutations in *Chlamydomonas reinhardtii* confer altered sensitivities to microtubule inhibitors and herbicides by enhancing microtubule stability. *J Cell Biol* 113, 605–614.
- Skillman KM, Diraviyam K, Khan A, Tang K, Sept D, Sibley LD (2011). Evolutionarily divergent, unstable filamentous actin is essential for gliding motility in apicomplexan parasites. *PLoS Pathogens* 7, e1002280.
- Sueoka N (1960). Mitotic replication of deoxyribonucleic acid in *Chlamydomonas reinhardtii*. *Proc Natl Acad Sci USA* 46, 83–91.
- Tapley EC, Starr DA (2013). Connecting the nucleus to the cytoskeleton by SUN–KASH bridges across the nuclear envelope. *Curr Opin Cell Biol* 25, 57–62.
- Umen JG, Goodenough UW (2001). Control of cell division by a retinoblastoma protein homolog in *Chlamydomonas*. *Genes Dev* 15, 1652–1661.
- Vandekerckhove J, Deboben A, Nassal M, Wieland T (1985). The phalloidin binding site of F-actin. *EMBO J* 4, 2815–2818.
- Wang Y (2005). The mechanism of cortical ingression during early cytokinesis: thinking beyond the contractile ring hypothesis. *Trends Cell Biol* 15, 581–588.
- Warren DT, Andrews PD, Gourlay CW, Ayscough KR (2002). Sla1p couples the yeast endocytic machinery to proteins regulating actin dynamics. *J Cell Sci* 115, 1703–1715.
- Wesolowska N, Machado P, Geiss C, Kondo H, Mori M, Schwab Y, Lenart P (2018). An F-actin shell ruptures the nuclear envelope by sorting pore-dense and pore-free membranes in meiosis of starfish oocytes. *BioRxiv*. <https://doi.org/10.1101/480434>.
- Wetzel DM, Håkansson S, Hu K, Roos D, Sibley LD (2003). Actin filament polymerization regulates gliding motility by apicomplexan parasites. *Mol Biol Cell* 14, 396–406.
- Wilson NF, Foglesong MJ, Snell WJ (1997). The *Chlamydomonas* mating type plus fertilization tubule, a prototypic cell fusion organelle: isolation, characterization, and *in vitro* adhesion to mating type minus gametes. *J Cell Biol* 137, 1537–1553.
- Zheng SQ, Palovcak E, Armache J-P, Verba KA, Cheng Y, Agard DA (2017). MotionCor2: anisotropic correction of beam-induced motion for improved cryo-electron microscopy. *Nat Methods* 14, 331–332.